

# Riser Interference and VIV Amplification in Tandem Configuration

E. Fontaine\*

IFP, Rueil-Malmaison, France

J. P. Morel

IFREMER, Plouzané, France

Y. M. Scolan

Ecole Supérieure d'Ingénieurs de Marseille, Marseille, France

T. Rippol

Oceanide, BGO-FIRST, La Seyne/Mer, France

**Wake Induced Oscillations (WIO) and amplification of Vortex Induced Vibration (VIV) are studied for 2 risers in tandem configuration. The criticality of riser interference is first investigated in term of nondimensional numbers for different types of risers. Theoretical, numerical and experimental approaches are then used simultaneously to define similarity rules and to investigate scale effects with respect to the Reynolds number. Finally, experimental results demonstrating amplification of VIV are given.**

## NOMENCLATURE

- $C_d$ : drag coefficient (also  $C_{d_i}$ )  
 $C_V$ : Cauchy number ( $C_V = (Ur)^2/\mu$ )  
 $D$ : riser diam ( $D_i$  for riser number  $i$ )  
 $f$ : first natural frequency (and associated pulsation  $\omega$ )  
 $i$ : subscript to identify riser number  
 $K$ : structural stiffness of 1st mode  
 $K_c$ : contact stiffness between risers  
 $L$ : initial spacing between risers  
 $M$ : riser mass per unit length in air including internal fluid (also defined as  $m_i$ )  
 $ma$ : fluid added mass per unit length ( $ma_i = \pi\rho D_i^2/4$ )  
 $Sc$ : Scruton number (also noted  $A_R$ )  
 $\tau$ : first natural period of riser  
 $Ur, V_R$ : reduced velocity ( $Ur = V_0/\omega \cdot D, V_R = 2\pi Ur$ )  
 $V(z)$ : current profile  
 $V_0$ : effective current velocity  
 $X_i$ : position of riser  $i$   
 $(x, y, z)$ : coordinate system ( $z$  is vertical downward)  
 $\rho$ : water density  
 $\psi_n(z)$ : modal shape associated to structural mode number  $n$   
 $\mu$ : reduced mass ( $\mu = 4m/\pi\rho D^2$ )  
 $\zeta_{x, drag}$ : hydrodynamic damping due to drag in  $x$  direction  
 $\zeta_i$ : structural damping of riser  $i$   
 $\zeta$ : total damping (structural and hydrodynamic)  
 $\tau$ : nondimensional time ( $\tau = \omega \cdot t$ )

## INTRODUCTION

Hydrodynamic riser interference is becoming a crucial issue as offshore technology moves into deep and ultra-deep water. The

main concern about riser interference is to be able to predict the risk of collision between closely spaced risers, and eventually to design risers able to withstand possible impact with each other. Besides turbulence buffeting, hydrodynamic interference between risers can be classified in 2 categories: Wake Induced Oscillation (WIO) and Vortex Induced Vibration (VIV).

WIO, also referred to as galloping, is a classical type of instability; see e.g., Blevins (1977, 1990, 2004) and Axisa (2001) for a simplified description of the mechanism underlining the phenomenon. Basically, spatial variations of the time-averaged hydrodynamic coefficients (lift and drag) can create such instability at high reduced velocity. WIO is a low-frequency motion which arises at the first natural period of the riser. Large amplitude, which may rise up to several tens of diam, is predicted (e.g., Wu, 2001).

VIV is known to be a self-limited motion with a maximum order of 1 diam for a single riser. However, in cylinder array, measurements have shown VIV amplification of up to 2 diam. VIV frequencies may be high as they are closely correlated with current velocity through a Strouhal relationship.

A literature survey indicates that hydrodynamic riser interference has been investigated recently, e.g., by Wu (2001) and Blevins (2004). A recommended practice RP F-203 is expected to be issued by DNV, as a result of Norwegian Deepwater Program research. Clearly, the next stage consists in better understanding the hydrodynamic loads acting on a riser placed in the wake of an upstream riser.

## CRITICALITY OF RISER INTERFERENCE IN DEEP AND ULTRA-DEEP WATER

In ultra-deep water, the first natural period of the riser is generally of the order of 50 to 100 s (Table 1), and the modal stiffness associated with the first natural frequency of the riser at midspan is very low, due to the riser length. Consequently, large displacements of the WIO type are likely to occur and must thus be studied. When the instantaneous distance between risers gets

\*ISOPE Member.

Received August 10, 2005; revised manuscript received by the editors December 14, 2005. The original version (prior to the final revised manuscript) was presented at the 15th International Offshore and Polar Engineering Conference (ISOPE-2005), Seoul, June 19–24, 2005.

KEY WORDS: Riser interference, clashing, VIV amplification.

below 3 to 4 diam, the upstream riser may attract the downstream one due to negative drag coefficient, leading to possible contact. Deep-water developments involve a large number of risers and umbilicals. The spacing between these components is then of critical importance. The amplitude of WIO has to be considered when performing a clearance analysis, not only for vertical risers, but also between adjacent jumpers or catenary risers, for which the first mode motion, of the so-called swinging rope type, has very low stiffness. The criticality of riser interference is first studied in terms of nondimensional numbers. Reduced velocity  $V_R = V_0/(f \cdot D)$  and Scruton number  $Sc = A_R = (2\pi m \zeta)/(\rho D^2)$  have been evaluated for various types of risers: Top Tension Risers (TTR), Steel Catenary Risers (SCR), Hybrid Catenary Risers (HCR), Composite (carbon fiber) and Drilling Risers, for some production or drilling configurations in depths from 600 to 2300 m. Results are summarized in Table 1. The reduced mass is defined as the ratio between the linear structural mass and the displaced mass of water. The first natural period is computed using the FEM DeepLines™ riser analysis software package. The reduced velocity is computed based on the effective velocity  $V_0$ , i.e., accounting for the modal shape function  $\psi_n(z)$  depending on the riser type:

$$V_0 = \left( \frac{\int V^2(z) \cdot \psi_n(z) \cdot dz}{\int \psi_n^2(z) \cdot dz} \right)^{1/2} \quad (1)$$

For vertical risers, a sinusoidal shape function is generally assumed. A typical value of 0.4 m/s for the effective velocity is obtained for the cases studied, although other data suggest values as high as 1.2 m/s in northern Norway. The Cauchy number is defined as the reduced velocity squared divided by reduced mass, i.e.,  $C_y = (Ur)^2/\mu$ . As will be seen in the simplified modeling, the Cauchy number indicates the magnification factor to be applied to the spatial variations of the hydrodynamic coefficients. The higher the Cauchy number, the higher the WIO motions, hence the risk of collision. Damping estimation is of crucial importance, as this effect will prevent instabilities from arising. Since the reduced velocity is high, hydrodynamic damping can be estimated theoretically (e.g., Blevins, 1990, 2004) by a 1st-order expansion:

$$\zeta_{x, \text{drag}} = \frac{1}{4\pi} \frac{V_0}{fD} \frac{\rho D^2}{m} Cd, \quad \zeta_{y, \text{drag}} = \frac{1}{2} \zeta_{x, \text{drag}} \quad (2)$$

for the  $x$  and  $y$  direction, respectively, due to incoming flow. Numerical predictions of damping coefficient are performed from free decay tests, either starting from slightly disturbed static equilibrium, or after a periodic regime has been established. Both methods lead to results similar to Eq. 2.

Stability analysis is classically performed using these nondimensional numbers, i.e., plotting the reduced velocity versus the Scruton number. As the damping coefficient varies linearly with

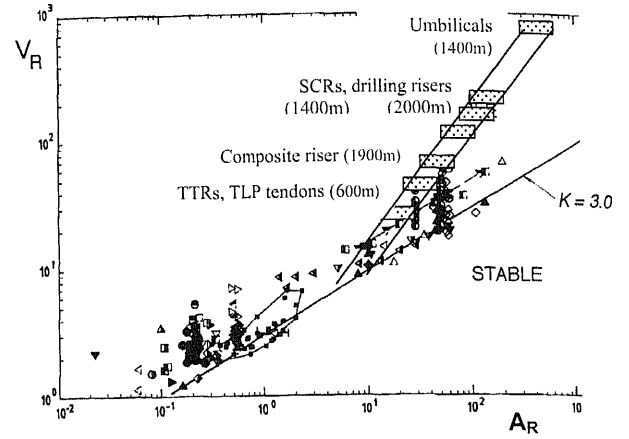


Fig. 1 Stability diagram used to design heat exchangers, symbols = stability criteria derived experimentally

reduced velocity (Eq. 2), it is then expected that the data points representing risers should lie on a straight line in the plot  $(A_R, V_R)$ , as can be seen in Fig. 1. The results are also compared with existing experimental data for heat exchangers. Indeed, the hydrodynamic phenomenon leading to galloping instabilities, or WIO, has been largely studied for nuclear power plants. It should be remembered that heat exchangers are formed by closely spaced cylinder arrays, the spacing being of the order of 1 cylinder diam. Still, results clearly indicate that riser interference phenomena may arise in deep and ultra-deep water, as most configurations are found to be unstable if the shielding effect is too strong and spacing between risers too small. This graph explains the recent efforts that have been made to better understand riser interference, e.g., Sagatun, Herfjord and Holmas (2002), Allen and Henning (2003), Kalleklev, Mork and Sodahl (2003), and Blevins (2004).

## WIO MODELING FOR BASIN TESTING: RISERS IN TANDEM

### Mathematical Model

WIO are classically studied using strip theory together with modal decomposition, leading to a 2-degree-of-freedom equivalent dynamic system. Fig. 2 illustrates the dynamics of 2 cylinders elastically supported in tandem. Using as a basis the model proposed by Blevins (1977, 2004) and Wu (2001), and taking into account different diam  $D_i$ , added mass  $(\rho \pi D_i^2/4)$  and structural damping coefficients  $\zeta_i$  leads to Eq. 3. Flow-effective velocity ahead of the cylinders  $V_0$  and wake velocity  $U(x)$  downstream of the front cylinder are considered.  $U(x)$  is based on the turbulent wake expression of Schlichting (Eq. 4). This set of equations is transformed by use of the nondimensional parameters given in Eq. 5. In case of contact between the cylinders, a spring force based on the riser surface elasticity is added in the right-hand side of Eq. 6. When the drag coefficient is known as a function of the position, these equations can easily be integrated numerically. As WIO result from static changes of lift and drag coefficients with respect to position (Eq. 6), special care has to be given to the hydrodynamic loading acting on the riser. The models described by Wu (2001) and Blevins (2004) are based on the Schlichting and Huse (1993) analytical formulation of the flow field, which is valid for large  $L/D$ . Little information is given about the hydrodynamic loads acting on the cylinders for small spacing, in particular when negative drag is observed on the downstream cylinder. Further, drag coefficients  $Cd_1(X)$  and  $Cd_2(X)$  on cylinders

UFR type	Depth (m)	OD (m)	$\mu$	$T_1$ (s)	$V_R$	$C_Y$	$Sc$
TTR Production	660	0.27	2.33	16	48	1E3	28.6
TTR Drilling	660	0.53	2.21	22	34	5E2	20.3
TLP Tendon	660	0.61	0.98	15	20	4E2	11.8
SCR Production	1300	0.5	1.34	95	150	17E3	89.6
Umbilical gas inj.	1300	0.1	2.5	58	567	13E4	340
Composite riser	2000	0.32	1.3	54	134	14E3	80.5
TTR Drilling	2300	1.4	1.06	150	100	10E3	49.6

Table 1 Main parameters governing WIO

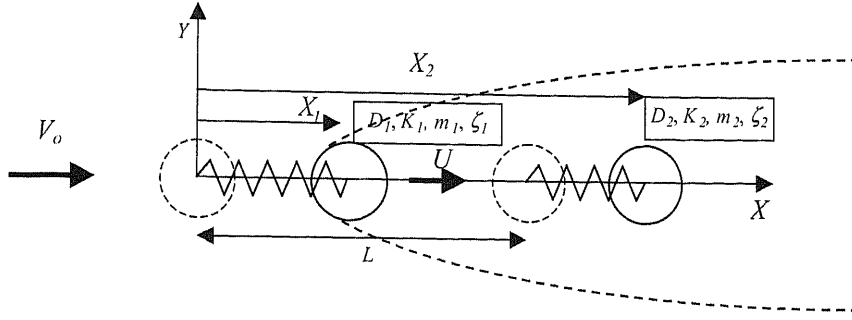


Fig. 2 Mathematical model definitions

$$\begin{cases} \ddot{x}_1 + 2\zeta_1\omega_1\dot{x}_1 + \omega_1^2x_1 = \frac{\rho V_0^2 D_1}{2(m_1 + ma_1)} Cd_1 \left( X_2 - X_1 + \frac{L}{D_1} \right) \left( 1 - \frac{\dot{x}_1}{V_0} \right) \left| 1 - \frac{\dot{x}_1}{V_0} \right| \\ \ddot{x}_2 + 2\zeta_2\omega_2\dot{x}_2 + \omega_2^2x_2 = \frac{\rho V_0^2 D_2}{2(m_2 + ma_2)} Cd_2 \left( X_2 - X_1 + \frac{L}{D_1} \right) \left( 1 - \frac{\dot{x}_2}{U} \right) \left| 1 - \frac{\dot{x}_2}{U} \right| \end{cases} \quad (3)$$

$$\bar{U} = \frac{U}{V_0} = \frac{U(X_2 - X_1 + L/D_1)}{V_0} = \left( 1 - \sqrt{\frac{Cd_1(X_2 - X_1 + L/D_1)}{(X_2 - X_1 + L/D_1) + 4/(Cd_1(X_2 - X_1 + L/D_1))}} \right) \quad (4)$$

$$\tau_i = \omega_i t, \quad X_i = \frac{x_i}{D_i}, \quad Ur_i = \frac{V_0}{\omega_i D_i}, \quad a_i = \frac{2(m_i + ma_i)}{\rho D_i^2}, \quad \Delta X_c = \frac{D_2 + D_1}{2D_1} - X_2 + X_1 - \frac{L}{D_1} \quad (5)$$

$$\begin{cases} \ddot{X}_1 + 2\zeta_1\dot{X}_1 + X_1 = \frac{Ur_1^2}{a_1} Cd_1 \left( X_2 - X_1 + \frac{L}{D_1} \right) \left( 1 - \frac{\dot{X}_1}{Ur_1} \right) Abs \left( 1 - \frac{\dot{X}_1}{Ur_1} \right) - \frac{Kc}{K_i} \Delta X_c \\ \ddot{X}_2 + 2\zeta_2\dot{X}_2 + X_2 = \frac{Ur_2^2 D_2}{a_2 D_1} Cd_2 \left( X_2 - X_1 + \frac{L}{D_1} \right) \left( 1 - \frac{\dot{X}_2}{\bar{U} Ur_2} \right) Abs \left( 1 - \frac{\dot{X}_2}{\bar{U} Ur_2} \right) + \frac{Kc}{K_i} \Delta X_c \end{cases} \quad (6)$$

in tandem depend on their relative position and on the Reynolds number (Figs. 3 and 4), hence the need to assess a proper scaling procedure.

### Rules

The mathematical model also allows us to derive similarity rules based on conservation of nondimensional numbers arising in the equations. In order to get the same values of  $X_1(t)$  and  $X_2(t)$  at full or at model scale, the following parameters shall be kept constant:

$$(Ur_1)_m = (Ur_1)_r \quad (7)$$

$$(\bar{U} \cdot Ur_2)_m = (\bar{U} \cdot Ur_2)_r \quad (8)$$

$$\left( \frac{Ur_i^2}{a_i} Cd_i \right)_m = \left( \frac{Ur_i^2}{a_i} Cd_i \right)_r \quad (9)$$

where:

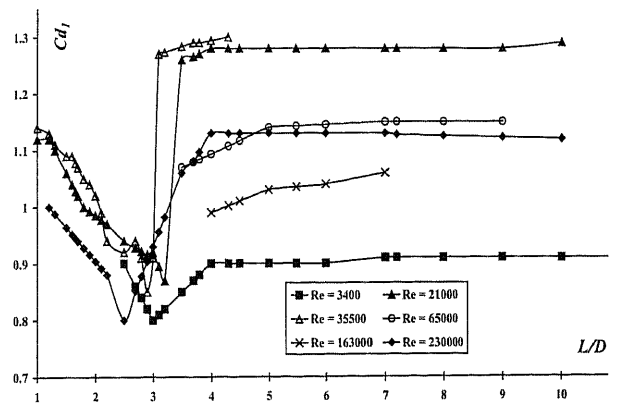
$$\frac{Ur_i^2}{a_i} Cd_i = \frac{\rho V_0^2 Cd_i}{2K_i} \quad (10)$$

and subscripts  $m$  and  $r$  refer to model and real configuration, respectively. Hydroelastic instabilities such as WIO and VIV amplification are studied experimentally in the IFREMER Circulating Water Channel at Boulogne/Mer on pivoting rods at 2-m water depth (Morel et al., 2003), and in the BGO-FIRST Wave-Current tank managed by Oceanide at La Seyne/Mer on cylindrical rods at 6- to 15-m water depth. Models are at about 1/10 and

1/100 scale, respectively. In these basins, water velocity ranges from 0.1 to 1 m/s, keeping good flow quality. At full scale, the Reynolds number typically ranges from 20,000 to 500,000 depending on the riser type, thus corresponding to a range from 1,000 to 50,000 at model scale.

### Hydrodynamic Coefficients Versus Reynolds Number

In order to investigate Reynolds effects, a database has been collected through a literature survey (Fontaine et al., 2005). Figs. 3 and 4 present plots of  $Cd_1$  and  $Cd_2$  as a function of the cylin-


 Fig. 3 Cylinders in tandem: front drag coefficient as function of spacing  $L/D$  and  $Re$

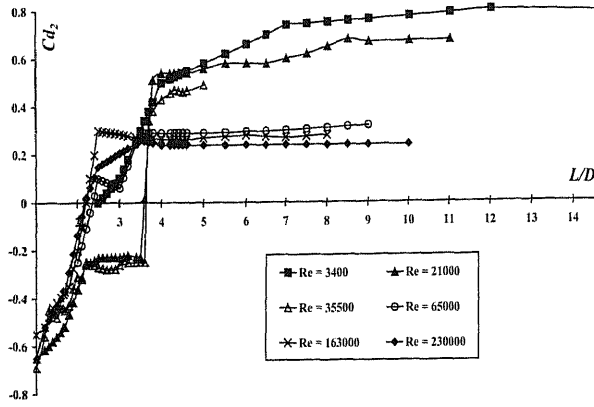


Fig. 4 Cylinders in tandem: rear drag coefficient as function of spacing  $L/D$  and  $Re$

der spacing  $L/D$  and the Reynolds number. When the spacing gets below a value of 3 to 4, a significant drop in drag coefficients occurs on both cylinders. Then the upstream cylinder drag increases when the spacing gets reduced, while the downstream cylinder drag still decreases to reach negative values, thus the attracting effect from the front riser. The Reynolds effect in the range mentioned above affects the drag coefficients significantly, a large spacing by factors which may reach 1.4 on the upstream cylinder and 4 on the downstream one.

The mathematical model describing the dynamics of 2 cylinders in tandem requires as input a mapping of the drag coefficient. Experimental values have thus been fitted analytically:

$$\begin{cases} Cd = \beta(Re) + \frac{\gamma(Re)}{L/D + \alpha} & L/D > (L/D)_c(Re) \\ Cd = a(Re) + b(Re)L/D & L/D \leq (L/D)_c(Re) \end{cases} \quad (11)$$

where  $(L/D)_c$  is the critical distance before  $Cd$  values drop. Figs. 5a and b show the variation of the values of  $Cd_1$  and  $Cd_2$  due to the Reynolds effect at model scale and at full scale. The minimum Reynolds number at full scale corresponds to the minimum one at model scale. Consequently one may have to consider that the drag on the front riser model may be underestimated by a factor of about  $0.5/1.3 \approx 0.4$  at large  $L/D$  for the minimum Reynolds cases.

**Example of 2 Cylinders in Tandem**

As an example, Fig. 6 shows the unsteady motion of 2 cylinders with equal diam in tandem configuration. The initial spacing is

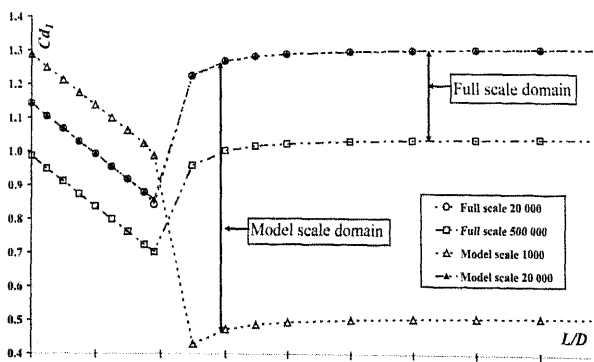


Fig. 5a Front cylinder: effect of test scaling on drag coefficient

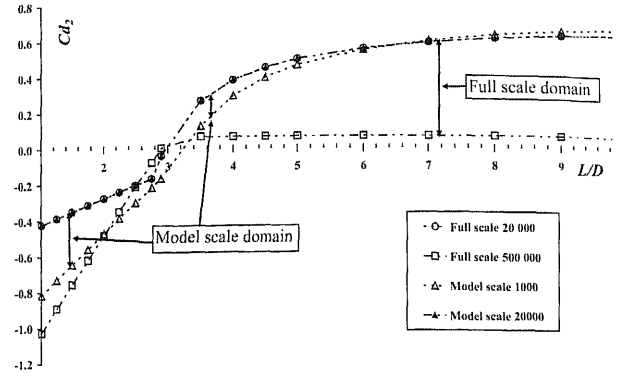


Fig. 5b Rear cylinder: effect of test scaling on drag coefficient

15 diam, the first natural period is of the order of 100 s, and the current effective velocity increases up to 0.4 m/s by steps of 0.02 m/s. Varying  $V_0$  and consequently  $Ur$  allows the prediction of clashing theoretical onset criteria. The front riser moves backward more than the rear one. When  $V_0$  reaches about 0.36 m/s, the gap between the risers becomes less than 3 diam, and the rear riser is attracted by the front one (since  $Cd_2 < 0$ ). Contact and bouncing still persist until the current speed drops sufficiently due to the time delay of the front riser motion with respect to the input.

**Model Testing Case: Application of Rules Accounting for Reynolds Effect**

One considers the riser configuration presented above at a  $\lambda = 1/33$  scale in an effective current velocity of 0.225 m/s.

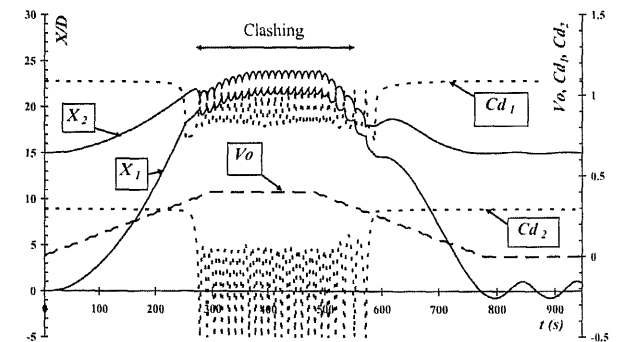


Fig. 6 Motion and drag coefficients for 2 risers in tandem in variable current  $v_0(t)$

Parameters		Full scale $Re \sim 110000$	1/33 Model accounting for Reynolds effect ( $Re \sim 4400$ )	1/33 Model without accounting for Reynolds correction
Upstream riser	$Cd_1$	1.135	1.0	1.0
	$fn_1$	0.01	0.48	0.48
	$K_1/m$	2.1	3.4	3.8
Downstream riser	$a_1$	3.7	3.3	3.7
	$Cd_2$	0.45	0.71	0.71
	$U/V_0$	0.75	0.77	0.77
	$fn_2$	0.01	0.49	0.48
	$K_2/m$	2.1	6.0	3.8
	$a_2$	3.7	5.6	3.7

Table 2 WIO parameters at full and model scale

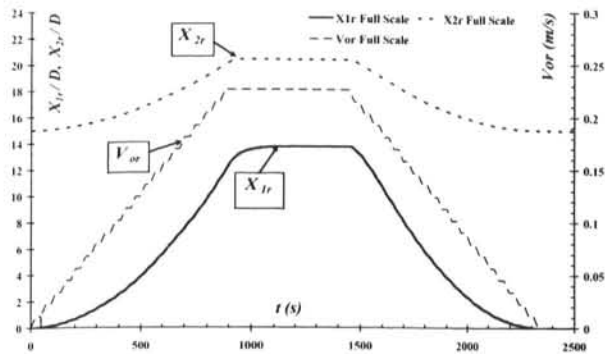


Fig. 7a Time evolution for displacement at full scale

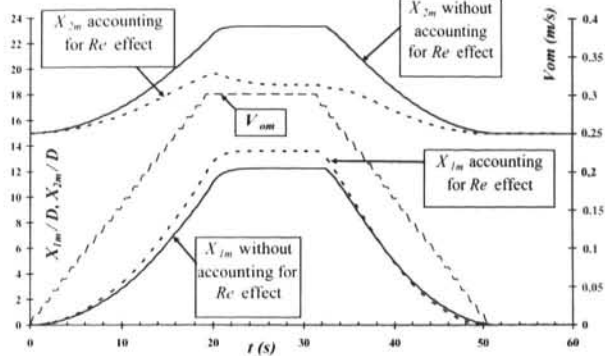


Fig. 7b Time evolution for displacement at model scale, with and without Reynolds correction

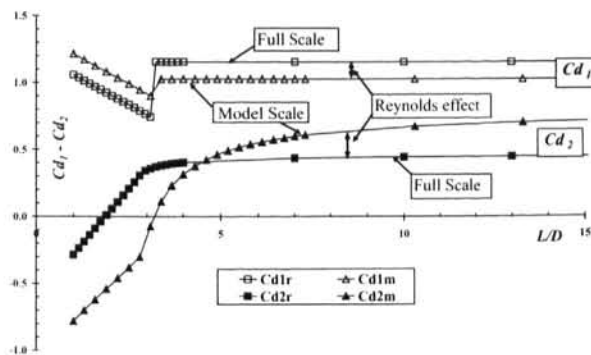


Fig. 8 Predicted spatial evolution of drag coefficient at full and model scale

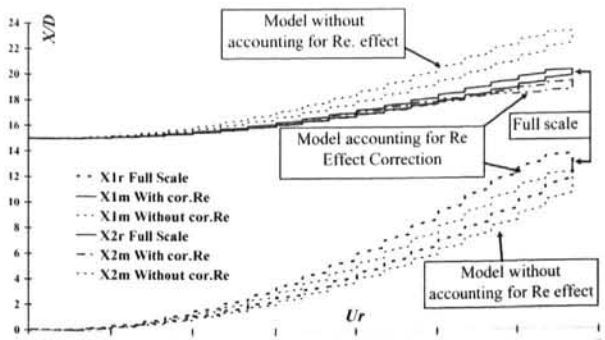


Fig. 9 Comparison of displacements at full and model scale with and without Reynolds correction

Taking care of the Reynolds influence between full scale and model scale at large  $L/D$  spacing, the natural frequencies and the support stiffness of the experimental pivoting rod (Morel et al., 2003) are computed using rules defined in Eqs. 7~10, and choosing a selected basin velocity  $V_{0m} \approx 0.3$  m/s. Accounting for the Reynolds effect on  $Cd$  values for both risers implies some variation of the stiffness  $K_1$  between the front and rear risers, according to Eq. 10. The stiffness  $K_2$  and the mass criteria  $a_2$  of the downstream riser are significantly changed to compensate for coefficient variation ( $Cd_2$ ), due to the Reynolds effect (Table 2). If the

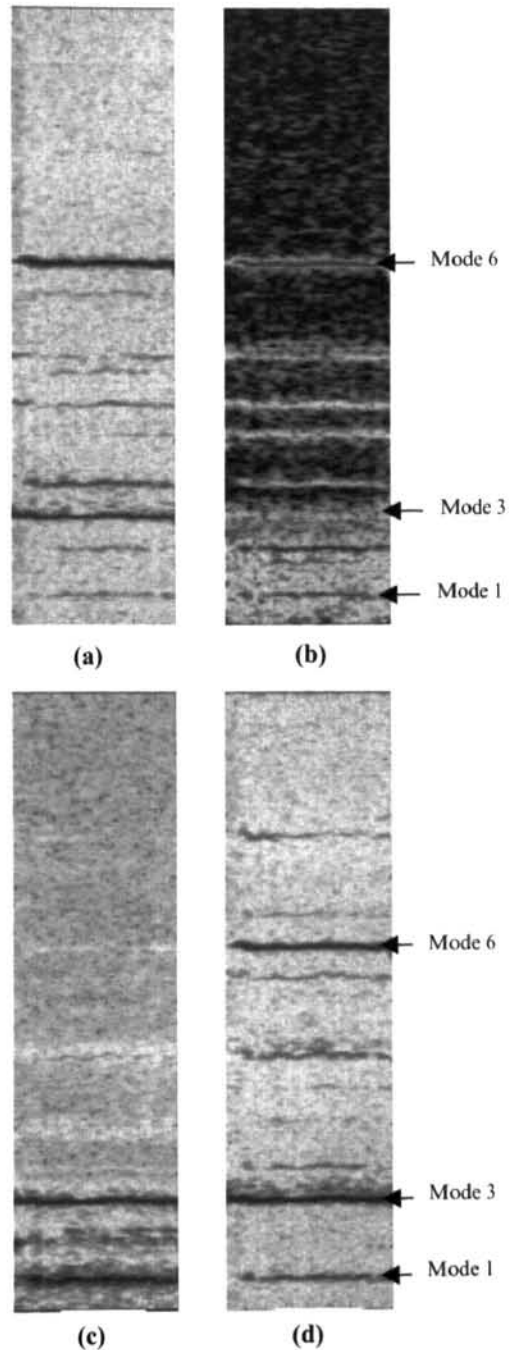


Fig. 10 Frequency versus Time for (a) inline reconstructed displacement  $X$ , (b) acceleration  $d^2X/dt^2$ , (c) cross-flow reconstructed displacement  $Y$ , (d) acceleration  $d^2Y/dt^2$  indicating fully developed statistically steady vibrations

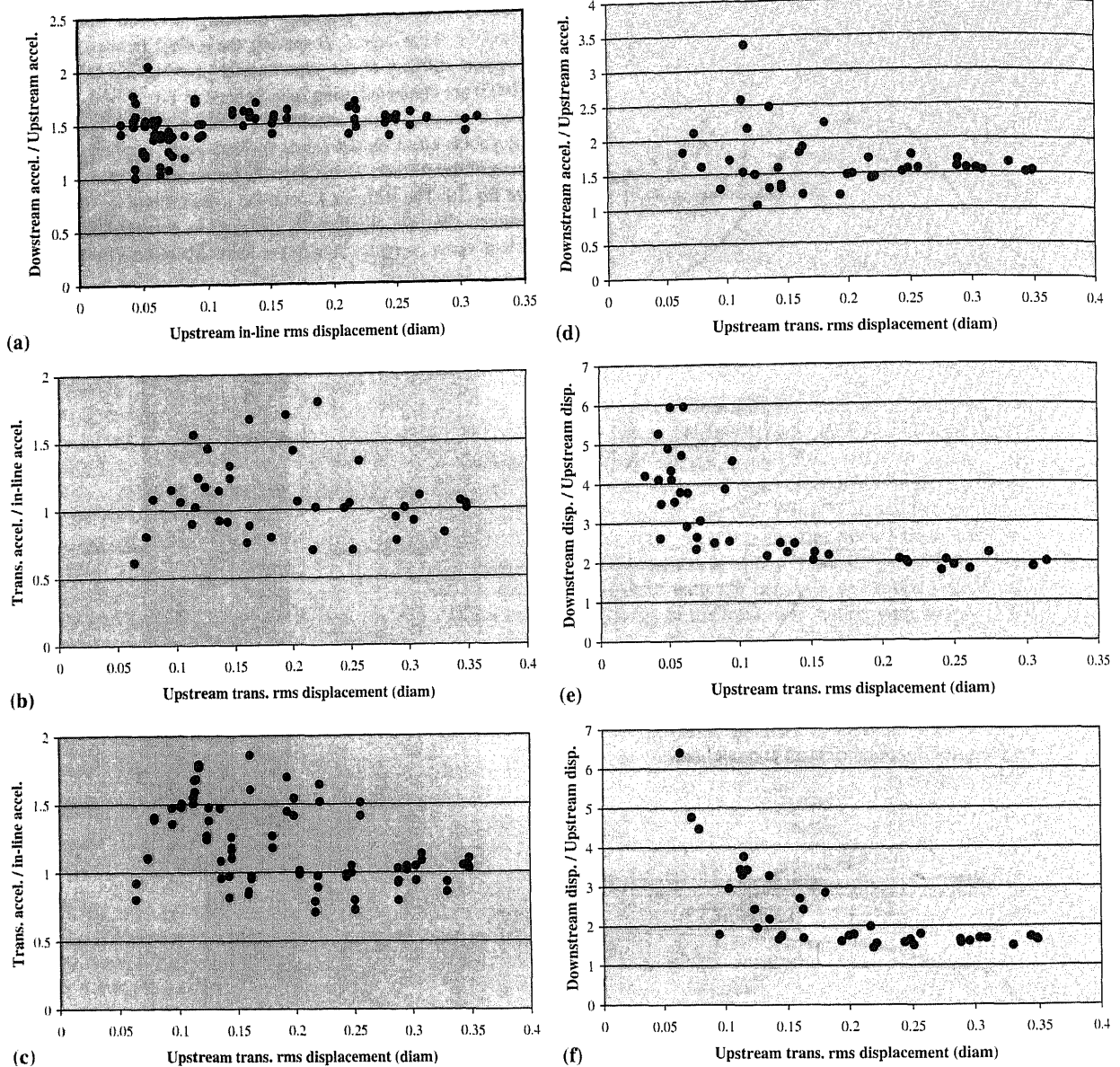


Fig. 11 Uniform flow: (a) Downstream cylinder in-line acceleration/upstream cylinder in-line acceleration versus upstream in-line rms displacement; (b) upstream cylinder-transverse accelerations/in-line accelerations versus upstream transverse rms displacement; (c) downstream cylinder-transverse accelerations/in-line accelerations versus upstream transverse rms displacement; (d) downstream cylinder transverse acceleration/upstream cylinder transverse acceleration versus upstream transverse rms displacement; (e) downstream cylinder in-line displacement/upstream cylinder in-line displacement versus upstream in-line rms displacement; (f) downstream cylinder transverse displacement/upstream cylinder transverse displacement versus upstream in-line rms displacement

Reynolds effect is not accounted for,  $Cd_i$  and  $\bar{U}$  can be deleted in Eqs. 8 to 10, and both models have the same stiffness and mass.

Figs. 7a and b present the time evolution of the displacements for full-scale and model test configurations of a riser tensioned by buoyancy cans. In the latter case, the Reynolds effect as defined previously is shown. Fig. 8 presents drag coefficients at full and model scale. Fig. 9 summarizes the displacement responses as a function of reduced velocity  $Ur$ .

As rules are used to scale the experiment, it is important to check if biases are not introduced in the process, leading to non-conservative results. At full scale, for the maximum current velocity of 0.225 m/s, the front riser moves backward by approximately  $14D$  and the rear one by  $5D$ , according to the modeling (Fig. 7a).

The relative distance between the 2 risers stays around  $6D$ , above the critical value of  $3D$  to  $4D$  at which the front riser starts to attract the rear one.

At model scale, if the Reynolds effect is not accounted for, the front riser moves approximately by only  $12D$ , and the rear riser motion is increased to about  $8D$  (Fig. 7b), due to the larger values of the drag coefficient at model scale (Fig. 8). The relative distance stays above  $11D$ , and the criticality of the configuration is not exhibited. Instead, if the Reynolds effect is accounted for on the model, the front riser motion remains identical to the full-scale one (Fig. 9). The motion of the rear riser is reduced to  $4D$  due to the variation of the drag coefficient (Fig. 8), which drops faster at model scale than at full scale for low  $L/D$ . The stage

where the front riser is starting to attract the rear one is reached earlier. Testing is then performed on a conservative basis.

## EXPERIMENTAL STUDIES OF VIV AMPLIFICATION

VIV amplification has been studied analytically (e.g., Facchinetti et al., 2002), numerically (Fontaine et al., 2003) and experimentally (Morel et al., 2003). New experiments have been performed in the BGO-FIRST tank on 2 closely spaced vertical risers clashing with each other at a 6-m water depth. Riser diam is 0.014 m and riser length is 8.6 m. Excitation by a slightly sheared current ranging from 0.14 to 0.38 m/s was produced over 1/3 of the riser length. Three accelerometers were used together with visual tracking (in the air and underwater) of targets disposed along the riser. Accelerometers were placed on the upstream riser at mid-depth, and on the downstream riser at mid- and quarter-depth from the free surface. Acceleration signals were integrated twice and filtered to find the displacement. Fig. 10 presents the time frequency analysis of the raw (acceleration) and reconstructed (displacement) signal, indicating well-established, statistically steady vibration. During the experiment, averaged dynamic tension varied from 160 to 200 N for the downstream cylinder and from 130 to 200 N for the upstream one.

Following Allen and Henning (2003), Figs. 11a~f plot variations of the acceleration and displacement ratios versus the upstream cylinder displacement. The purpose is to identify the thresholds above which amplification of the downstream cylinder motion may occur. These thresholds concern both the in-line and transverse displacements. All variables are calculated as rms quantities over the entire time series, excluding the starting and ending transient phases. For this set of data, the gap between the 2 cylinders is  $L/D = 3$ , which is in the critical range where drag coefficient on the downstream cylinder rapidly decreases. As a result, clashing was observed, with its frequency depending mainly on the intensity of the current. As expected, clashing increasingly occurs with the amplitude of the transverse displacement of the upstream cylinder.

In this experimental campaign, the measured transverse displacement of the upstream cylinder does not exceed  $D/3$ . Thresholds can be identified in terms of the upstream cylinder motion. Hence amplification may start when  $x_1/D \approx 0.1$  (Figs. 11a and e), and  $y_1/D \approx 0.2$  (Figs. 11d and f). It is worth noting that above these thresholds, the ratios of accelerations (in line or transverse) are roughly 1.5 (Figs. 11a and e). For the displacements, the ratio ranges from 1.5 to 2 for large displacements of the upstream riser (Figs. 11e and f). Hence the dynamic of the downstream cylinder is much more complex than that of the upstream cylinder.

Another asymmetry can be underlined by plotting the ratios of the acceleration components in the 2 planar directions. As illustrated in Figs. 11b and c, the transverse accelerations of both upstream and downstream cylinders are always greater than their respective in-line acceleration. For the present gap between cylinders, these results agree well with those of Allen and Henning (2003); in particular as the in-line motion of the upstream cylinder increases, the 2 components of the acceleration are roughly of the same magnitude (Figs. 11b and c).

## CONCLUSIONS AND PERSPECTIVES

Typical riser configurations for deep-water offshore drilling and production have been selected and for which similarity parameters related to the frequency response and the damping have been derived. Although this approach is conservative, plotting the nondimensional numbers in a stability diagram for heat exchanger

pipes at small spacing shows that riser configurations may become unstable due to WIO phenomena should the shielding effect be too strong or spacing too small.

Mathematical models describing WIO require mapping of hydrodynamic coefficients as a function of riser spacing, including the near field where negative drag is measured on the rear riser at low spacing. An experimental database from a literature survey has exhibited a significant influence on the spacing and on the Reynolds number as well. Correlation formulas from the database have been used for the development of a mathematical model of the dynamics of 2 risers in tandem, taking into account relative motion as in Wu (2001) and elastic bouncing when contact occurs. This permits the estimation of the current velocity at which contact occurs, as shown in an example.

Similarity laws taking into account the Reynolds effect on the wake velocity and the drag coefficients have been derived. For similarity to be satisfied on a pivoting rod at an initially large spacing, the stiffness and the mass need to be adjusted differently on both riser models. This is shown for a model at 1/33 scale. Then the front riser motion at model scale can be identical to the motion at full scale, and the rear one is on the conservative side as the drag coefficient drops faster at low spacing for low Reynolds numbers. Without accounting for the Reynolds effect, the front riser motion is decreased and the rear one increased, which gives too large a spacing estimate and a nonconservative testing procedure. This has to be considered either in the models' design or in the upscaling process of the basin results.

Experiments have been performed on 2 closely spaced vertical risers clashing at a 6-m water depth to assess the effect of VIV amplification. Experimental results indicate that the rms motion of the downstream cylinder can be more than twice as much that of the front cylinder.

## ACKNOWLEDGEMENTS

This paper is dedicated to Jean-Pierre Morel, Head of the IFREMER Applied Hydrodynamics Laboratory, who has been involved with riser array projects (among others) over the last 4 years. J. P. Morel, who retired in April 2005, has influenced young researchers especially in the field of experimental testing and the deriving of rules.

We also would like to acknowledge the financial support of TOTAL; P. Lespinasse, Riser Expert; and of the Comité d'Etudes Pétrolières et Marines (CEP&M), under contract CO 3007/04. The experimental campaign in BGO-FIRST is carried out within the network GIS-Hydro, financially supported by Conseil Général du Var.

## REFERENCES

- Allen, DW, and Henning, DL (2003). "Vortex-induced Vibration Current Tank Test of Two Equal-diameter Cylinders in Tandem," *J Fluids and Struct*, Vol 17, pp 767–781.
- Blevins, R (1977, 1990). *Flow-induced Vibration*, 1st and 2nd editions, Van Nostrand Reinhold Company.
- Blevins, R (2004). "Model for Forces on and Stability of a Cylinder in a Wake," *Proc Flow Induced Vibr Conf*, E de Langre, ed, Ecole Polytechnique, Paris.
- DeepLines™ (2005). *IFP/PRD Rept*, IFP.
- Facchinetti, M, et al. (2002). "VIV of Two Cylinders in Tandem Arrangement: Analytical and Numerical Modeling," *Proc*

- Int Conf Offshore and Polar Eng*, Kyushu, ISOPE, Vol 3, pp 524–531.
- Fontaine, E, et al. (2003). “VIV on Risers with Top-tensioned Buoyancy Cans—Part 1: Numerical and Simplified Analysis,” *Proc Int Conf Offshore and Polar Eng*, Honolulu, ISOPE, Vol 3, pp 608–614.
- Fontaine, E, Morel, JP, Scolan, YM, and Rippol, T (2005). “Riser Interference and VIV Amplification in Tandem Configuration,” *Proc Int Conf Offshore and Polar Eng*, Seoul, ISOPE, Vol 2, pp 226–233.
- Huse, E (1993). “Interaction in Deep-sea Riser Arrays,” *Proc Offshore Tech Conf*, Houston, Paper No 7237.
- Kalleklev, AJ, Mork, K, and Sodahl, N (2003). “Design Guide-line for Riser Collision,” *Proc Offshore Tech Conf*, Houston, OTC15383.
- Morel, JP, et al. (2003). “VIV on Risers with Top-tensioned Buoyancy Cans—Part 2: Experimental Modelling,” *Proc Int Conf Offshore and Polar Eng*, Honolulu, ISOPE, Vol 3, pp 615–622.
- Sagatun, SI, Herfjord, K, and Holmås, T (2002). “Dynamic Simulation of Marine Risers Moving Relative to Each Other Due to Vortex and Wake Effect,” *J Fluids and Struct*, Vol 16, No 3, pp 375–390.
- Wu, W, Huang, S, and Barltrop, N (2001). “Multiple Stable/unstable Equilibria of a Cylinder in the Wake of an Upstream Cylinder,” *Proc Conf Offshore Mech & Art Eng, OMAE/OFT-1170*.

## **Proceedings of the 6th (2005) ISOPE Ocean Mining Symposium** Changsha, Hunan, China, October 9–13, 2005

Exploration and survey, environment, mining systems and technology, processing,  
gas hydrates, and deep-ocean water upwelling

*The Proceedings* (ISBN 1-880653-65-6, 276 pp.; \$100 (ISOPE Member; \$80)) is available from ISOPE, P.O. Box 189, Cupertino, California 95015-0189, USA; Fax 1-650-254-2038; E-mail [orders@isope.org](mailto:orders@isope.org)